AIAA JOURNAL
Vol. 36, No. 10, October 1998

Nonclassical Dense Gas Flows for Simple Geometries

Brady P. Brown*
Krispin Technologies, Inc., Rockville, Maryland 20850-4304
and
Brian M. Argrow†
University of Colorado, Boulder, Colorado 80309-0429

Two-dimensional shock wave reflection and refraction phenomena for dense gases in the high pressure and density region near the thermodynamic critical point are compared and contrasted to shock phenomena over well-known configurations for dilute, perfect gases. Both transient and steady wave fields are simulated using a time-accurate, predictor-corrector total variation diminishing scheme that solves the Euler equations incorporating the van der Waals thermodynamic model. Detailed displays of wave field structure for both perfect gas and dense gas flowfields are shown. Nonclassical wave phenomena, such as disintegrating shocks, expansion shocks, and shock-fan composite waves for wedges, ramps, circular arcs, and other geometries, demonstrate significant differences in dense gas flowfields from those of perfect gases.

Nomenclature

a = speed of sound
b = van der Waals force parameter
c_v = specific heat at constant volume
$\boldsymbol{E}$ = streamwise flux vector
e = specific internal energy
$\boldsymbol{F}$ = transverse flux vector
n = temperature exponent
p = pressure
$\boldsymbol{Q}$ = conservative vector
R = gas constant
s = specific entropy
T = temperature
t = time
v = specific volume
x = streamwise spatial coordinate
y = transverse spatial coordinate
Z_c = critical compressibility
α = van der Waals covolume parameter
Γ = fundamental derivative of gas dynamics
γ = ratio of specific heats
δ = R/c_v
θ = turn angle
ρ = density

Subscripts

c = critical point
I = incident shock wave
r = ramp wall value
w = wedge wall value
0 = reference value
∞ = freestream value
- = nondimensional

Introduction

SOME heavy fluids may exhibit nonclassical phenomena in the single-phase vapor region near the thermodynamic critical point, i.e., the dense gas region.[1,2] Cramer[3] refers to these as BZT fluids to acknowledge the research contributions of Bethe,[4] Zel'dovich,[5] and Thompson.[6] Some of these fluids are currently used as heat transfer fluids and are characterized by large molecules with correspondingly large specific heats. Nonclassical flows of BZT fluids result from the nonmonotone variation of the Mach number with respect to density.[3,7,8] In a nonclassical flow, the second law of thermodynamics requires that compression shock waves cannot form, and if a compression shock enters the nonclassical region, it must disintegrate into a compression fan. Conversely, expansion waves may coalesce into expansion shock waves. Many in the aerospace field may find the dynamics of dense gases initially counterintuitive. For those, the present paper may serve as an introduction to nonclassical, dense gas flow phenomena.

Heavy fluids are currently used in a number of engineering applications such as heavy gas wind tunnels and organic Rankine cycle engines. For wind-tunnel applications, heavy fluids are used to produce relatively high-Reynolds-number flows with reduced plenum pressure, compared to lighter gases. References 7–13 present discussions of nozzles and wind-tunnel flows using dense gas models. Some turbomachinary designs take advantage of the high heat capacity of heavy fluids but evidently do not take advantage of nonclassical phenomena.[14,15]

Recent investigations of transonic aerodynamics for nonclassical flows show a substantial delay of the onset of supersonic flow over an airfoil with a corresponding increase in the critical Mach number.[16,17] Inviscid simulations of turbine cascade flows show improved efficiency for nonclassical flows through turbine cascades and channels.[18–20] This improved efficiency results from the reduction in strength or complete disintegration of compression shock waves, thus reducing wave drag.

The anomalous behavior of BZT fluids is explained through the second law of thermodynamics coupled with elementary shock theory.[4] The relationship between the entropy change and specific volume across a weak shock is written

$$\Delta s = -\left(\frac{\partial^2 p}{\partial v^2}\right)_s \frac{(\Delta v)^3}{12T} \tag{1}$$

where $(\partial^2 p/\partial v^2)_s$ measures the concavity of an isentrope. For dilute gases far from the critical point, we have condition 1,

$$\left(\frac{\partial^2 p}{\partial v^2}\right)_s > 0$$

requiring $\Delta v < 0$ to satisfy the second law. For thermodynamic regions where the concavity of the isentropes is reversed, condition 2 is

$$\left(\frac{\partial^2 p}{\partial v^2}\right)_s < 0$$

Presented as Paper 97-1881 at the AIAA 28th Fluid Dynamics Conference, Snowmass Village, CO, June 29–July 2, 1997; received July 28, 1997; revision received July 7, 1998; accepted for publication July 8, 1998.

*Research Scientist. Member AIAA.
†Assistant Professor, Department of Aerospace Engineering Sciences. Senior Member AIAA.

so that the specific volume v must increase across the shock wave to have a corresponding increase in Δs. This indicates that expansion waves will steepen into shocks and compression waves will spread into fans, i.e., the reverse behavior of flows having condition 1.

Using the van der Waals gas model, Bethe[4] and Zel'dovich[5] were the first to demonstrate thermodynamic regions that meet condition 2. Thompson[6] apparently was the first to recognize the importance of the sign of the single parameter Γ that governs the nonlinear dynamics of gases and called it the fundamental derivative of gas dynamics:

$$\bar{\Gamma} = -\frac{v}{2}\left[\left(\frac{\partial^2 p}{\partial v^2}\right)_s \Big/ \left(\frac{\partial p}{\partial v}\right)_s\right] = 1 + \frac{\rho}{a}\left(\frac{\partial a}{\partial \rho}\right)_s \qquad (2)$$

written here in nondimensional form. For convenience, the overbar is dropped from here forward. As indicated by the second formulation of Eq. (2), the fundamental derivative describes the rate of change of the convected speed of sound with density for a simple wave. For fluids having condition 1, $\Gamma > 0$ because the denominator in Eq. (2) $(\partial p/\partial v)_s < 0$ everywhere from the requirement of thermodynamic stability. The gas dynamics for the $\Gamma > 0$ region is said to exhibit positive nonlinearity. Negative nonlinearity occurs in the thermodynamic region where $\Gamma < 0$ because the curvature of the isentropes is reversed, i.e., condition 2. An example of an isentrope inflection and the corresponding $\Gamma < 0$ region is evident in the p–v diagram in Fig. 1. Thus, a fluid whose thermodynamic condition lies below the $\Gamma = 0$ line can exhibit flows where discontinuities exist as expansion shocks and compression waves spread as fans. Also, as indicated by the second formulation of Eq. (2), the speed of sound a necessarily increases in the $\Gamma < 0$ region as the density ρ decreases. Thus, with the present terminology a dense gas refers to a fluid that exhibits a single-phase vapor region with $\Gamma < 0$, i.e., the vapor phase of a BZT fluid.

Whether a fluid is predicted to have a $\Gamma < 0$ region above the saturation curve depends on the molecular weight and specific heat of the fluid in conjunction with the gas model used. Using several gas models, Thompson and Lambrakis[1] analytically show specific examples of hydrocarbons and fluorocarbons in which negative nonlinearity may be observed in the vapor phase. Cramer[2] confirms these findings and extends the list of BZT fluids to several other commercially available fluorocarbons.

The only experimental attempt to show single-phase, nonclassical dense gas phenomena is reported by Borisov et al.,[21] who observed what was believed to be expansion shocks in trifluorochloromethane ($CC1F_3$, Freon-13). However, their findings are questioned because simple calculations show that Freon-13 is not a BZT fluid, even with the van der Waals gas model, which overestimates the size of the $\Gamma < 0$ region.

As the preceding discussion indicates, most recent studies of the nonclassical gas dynamics of BZT fluids are primarily computational. This includes recent shock tube simulations of transient, one-dimensional dense gas wave fields by Argrow[22] and transient two-dimensional shock tube flows over various geometries by Brown and Argrow.[23] The work presented here is a continuation of this research to explore transient and steady dense gas flows for simple geometries. A goal of this research is the utilization of nonclassical aerodynamics in engineering applications, particularly for turbomachinary.

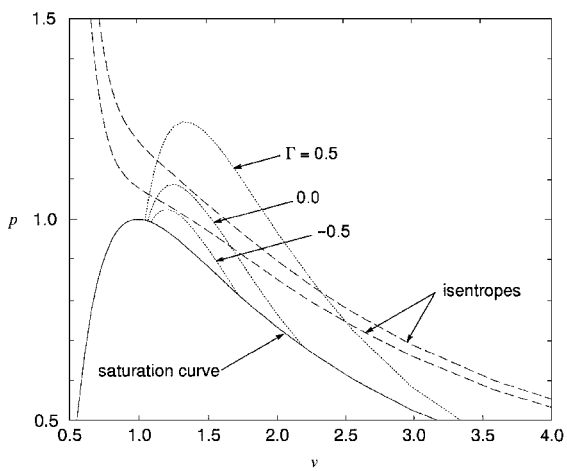

Fig. 1 Van der Waals model; p–v diagram showing the saturation curve, constant Γ contours, and two isentropes that pass through the $\Gamma < 0$ region.

Steady and unsteady shock wave reflection phenomena involving simple geometries for dilute, perfect gases are well documented. In contrast, due to the complexity of the state equations for dense gases, wave interactions in the dense gas regime are often not as intuitively predictable or understandable. Shock wave reflections in the dense gas regime can differ from those of a perfect gas because Γ may become negative in some regions of the flow. Because the region of negative nonlinearity is restricted to a finite range of temperatures and pressures, waves interacting with other waves or boundaries may cause Γ to change sign, resulting in regions of mixed nonlinearity.

The purpose of the present study is to demonstrate, through simulation and analyses of selected cases, some dense gas phenomena that may occur in nonclassical aero–gas dynamics. The presentation consists of a computational comparison of perfect gas and dense gas wave fields for two-dimensional unsteady and steady flows over simple geometries. A two-step total variational diminishing (TVD) scheme is used to solve the time-dependent, two-dimensional Euler equations of a van der Waals gas. Steady flow solutions are obtained in the conventional asymptotic limit of large time with steady flow boundary conditions. The wave field simulations include moving shocks incident upon geometries such as ramps and steps and steady flows over similar geometries.

Governing Equations and Numerical Method

The thermal equation of state is that of a van der Waals gas,

$$p = [\rho RT/(1 - b\rho)] - \alpha\rho^2 \qquad (3)$$

where α and b are the well-known van der Waals constants. The caloric state equation is

$$e = e_0 + c_v T - \alpha\rho \qquad (4)$$

where e_0 is a reference value. For a van der Waals gas, the specific heat $c_v(T)$ is simply the value in the dilute gas limit. The advantage of the van der Waals formulation is that it provides a model that is easily implemented into a numerical scheme and is computationally inexpensive compared with more complex gas models. Thus, it is used more for its simplicity than accuracy and is well suited to model the qualitative structure of dense gas wave fields.

Equations (3) and (4) can be written in reduced-variable form by nondimensionalizing p, ρ, and T by their values at the critical point and by naturally setting the compressibility factor at the critical point $Z_c = (p/\rho RT)_c = \frac{3}{8}$ so that

$$\bar{p} = \frac{8\bar{\rho}\bar{T}}{3 - \bar{\rho}} - 3\bar{\rho}^2 \qquad (5)$$

$$\bar{e} = (e - e_0)/RT_c = (\bar{T}/\delta) - \tfrac{9}{8}\bar{\rho} \qquad (6)$$

The overbar indicates nondimensional variables, and $\delta = R/c_v$. Note that the free parameters α and b have been eliminated. This indicates that all fluids satisfy the same state equation when reduced variables are used, which satisfies the principle of corresponding states, e.g., see Ref. 24. The variable specific heat is represented over the finite temperature range of interest by

$$\bar{c}_v(\bar{T}) = \bar{c}_v(1)\bar{T}^n \qquad (7)$$

where $n = 0.45$ is generally representative of heavy fluorocarbons.[1]

The compressible, inviscid flow is simulated by numerical solution of the two-dimensional, time-dependent Euler equations

$$\frac{\partial \boldsymbol{Q}}{\partial t} + \frac{\partial \boldsymbol{E}}{\partial x} + \frac{\partial \boldsymbol{F}}{\partial y} = 0 \qquad (8)$$

where the conservative state vector $\boldsymbol{Q}$ and the Cartesian flux vectors $\boldsymbol{E}$ and $\boldsymbol{F}$ are nondimensionalized with respect to the critical point values of the primitive variables.[23]

A predictor–corrector, TVD (PCTVD) scheme based on the Davis–Roe flux-limited method[25] is used to solve the nonlinear hyperbolic system in Eq. (8). This scheme is a conservative, pseudo finite volume method that is formally second-order accurate in time and space. The scheme is applied to the conservative system just as with a perfect gas, except the van der Waals equations of state, Eqs. (5) and (6), are employed. Four permutations of the predictor–corrector sequence are used to eliminate directional bias because the flowfields involve waves moving and interacting in several different directions. Reflective (solid wall) boundary conditions are implemented on the upper and lower boundaries for both transient and steady cases. For steady flows, the left boundary is treated as a uniform supersonic inflow and the right boundary as a supersonic outflow. For transient flowfields with moving shocks, the right boundary is solid, whereas conditions at the left boundary are set to the postshock values found from the Rankine–Hugoniot jump conditions. A complex, subsonic inflow condition is avoided by not allowing interior disturbances to reach the left boundary. Brown and Argrow[23] present a detailed error analysis of the PCTVD scheme. Their analysis includes a comparison to experimental interferogram data and a grid resolution and convergence study. Additional details of the PCTVD scheme applied to nonclassical flow simulations are presented in Refs. 13 and 22.

Results

Initial conditions for the transient cases are in Table 1, and freestream conditions for the steady flow cases are in Table 2. For the transient cases computed using the perfect gas model, initial conditions are normalized with values upstream of the shock for a gas with $\gamma = \frac{5}{3}$. The case with $\gamma = \frac{7}{5}$, shown subsequently, is an exception. Transient cases in the dense gas regime computed from the van der Waals model are normalized with critical point values. For steady flows, pressure p and density ρ are normalized to the freestream conditions for the perfect gas cases and to the critical point values for the dense gas cases. All dense gas cases use $\delta = 0.0125$, which is representative of heavy fluorocarbons.

In Figs. 2–15 wave fields for the density ρ are shown by isopycnic contours superimposed on a gray scale. Darker shades correspond to higher densities, as is evident in the scale plot of normalized density to the right of each figure. Densities for the perfect gas cases are normalized to the density upstream of the shock ρ_1 for transient cases and the freestream value ρ_∞ for steady cases. Densities for the dense gas cases are normalized to the critical point value ρ_c. The 20 contours are equally incremented between the highest and lowest values of density present in the wave field. Velocity vectors are also superimposed. The orientation and relative length of each arrow represents the direction and relative speed, respectively, of the fluid located at the tail of the arrow. For the dense gas cases, solid-white contours depict the $\Gamma = 0$ lines, whereas dashed-white contours correspond to a $\Gamma < 0$ value to indicate the negative Γ regions. Note that in most of the following comparisons of perfect gas and dense gas flowfields the incident and freestream Mach numbers are different. This is because the nonclassical flow regime is limited to transonic and low-subsonic Mach numbers.[8]

Table 1 Initial conditions for transient cases

Case	$\bar{p}_2$	$\bar{\rho}_2$	$\bar{v}_1$	$\bar{u}_2$	$\bar{p}_1$	$\bar{\rho}_1$	$\bar{v}_2$	$\bar{u}_1$
TP1	1.64	1.34	0.75	0.40	1.00	1.00	1.00	0.00
TP2	12.16	3.06	0.33	2.74	1.00	1.00	1.00	0.00
TD1	0.98	0.80	1.25	0.14	0.89	0.56	1.79	0.00
TD2	0.98	0.62	1.61	−0.14	1.09	0.88	1.14	0.00
TD3	1.01	0.85	1.18	0.64	0.58	0.28	3.57	0.00

Table 2 Freestream conditions for steady cases

Case	$\bar{p}_\infty$	$\bar{\rho}_\infty$	$\bar{v}_\infty$
SP1	1.00	1.00	1.00
SD1	1.09	0.88	1.14
SD2	0.98	0.62	1.61

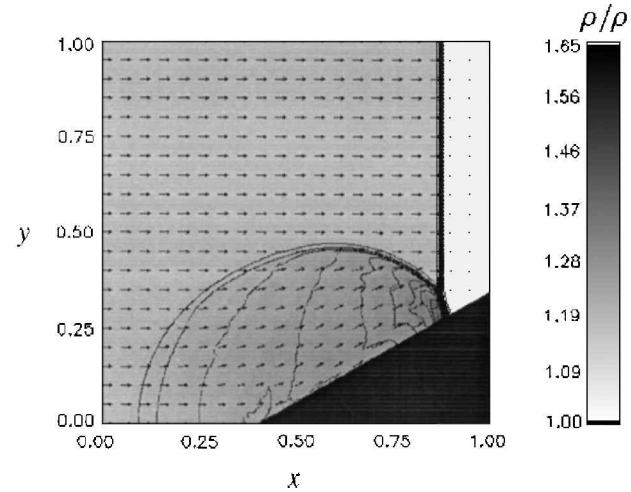

Fig. 2 Single Mach reflection for a perfect gas; $M_I = 1.23$, $\theta_w = 30$ deg, TP1 conditions.

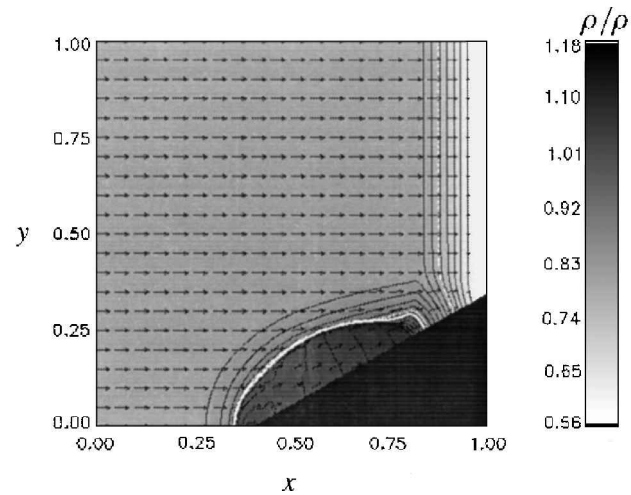

Fig. 3 Dense gas compression fan incident upon a $\theta_w = 30$ deg wedge; TD1 conditions.

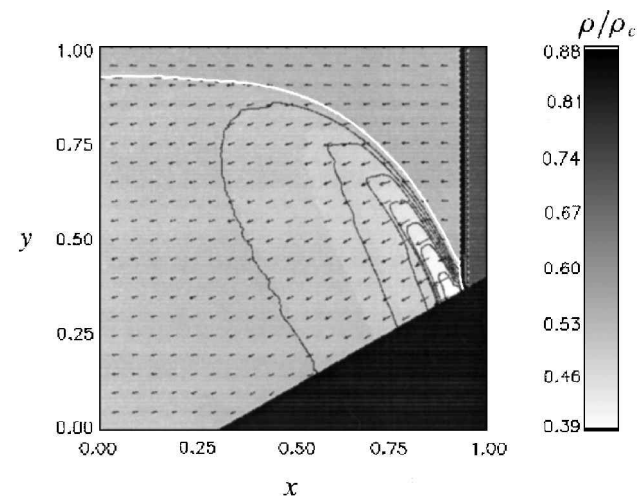

Fig. 4 Expansion shock incident upon a $\theta_w = 30$ deg wedge; $M_I = 1.05$, TD2 conditions.

Transient Flows

Figures 2–7 show cases for transient flowfields. The incident wave is started to the left of the obstacle and propagates to the right. Figure 2 shows the density field for a compression shock computed using the perfect gas model with the TP1 conditions. The shock is incident on a compressive wedge of angle $\theta_w = 30$ deg with a shock wave Mach number $M_I = 1.23$. As predicted by theory, the wave field configuration is a single Mach reflection. The Mach stem and reflected shock are well resolved. Because the shock is weak, the

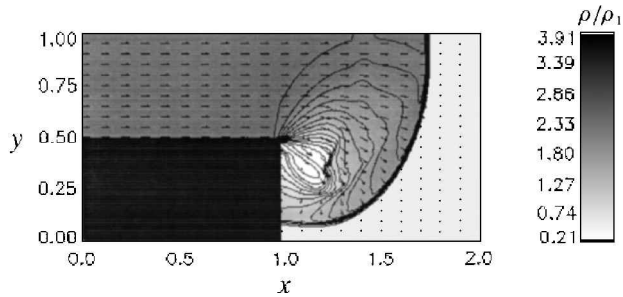

Fig. 5 Perfect gas shock diffracting over a backward-facing step; M_I = 3.2, TP2 conditions.

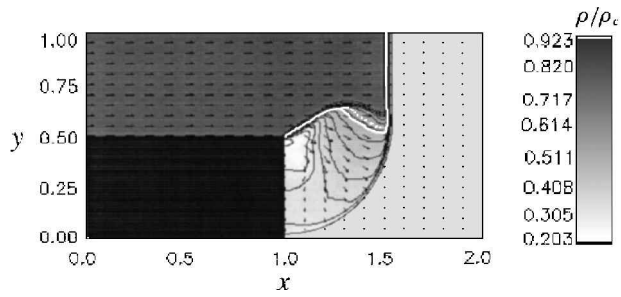

Fig. 6 Dense gas compression shock diffracting over a backward-facing step; M_I = 1.23, TD3 conditions.

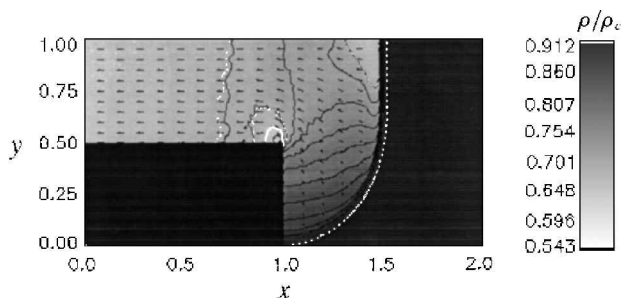

Fig. 7 Dense gas expansion shock diffracting over a backward-facing step; M_I = 1.05, TD2 conditions.

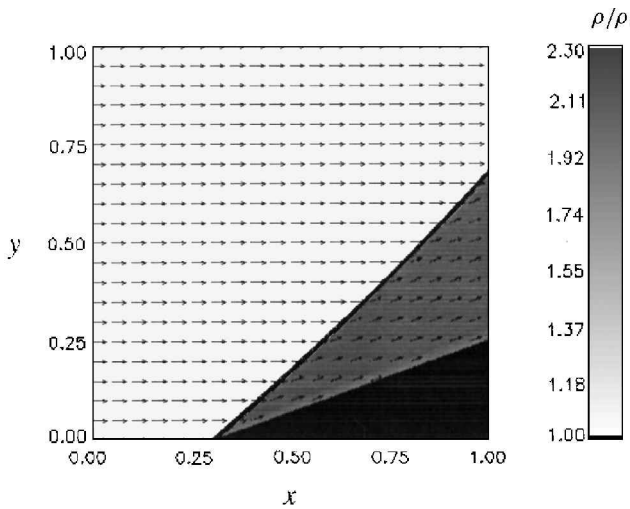

Fig. 8 Perfect gas attached oblique compression shock; M_∞ = 3.0, θ_w = 20 deg, SP1 conditions.

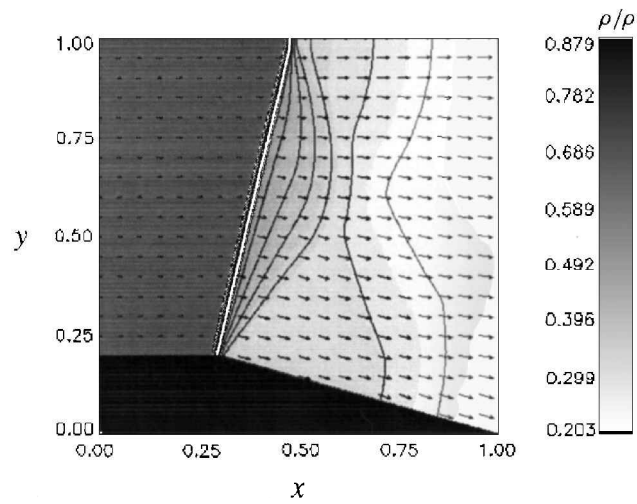

Fig. 9 Dense gas expansion shock–fan; M_∞ = 1.1, θ_w = − 20 deg, SD1 conditions.

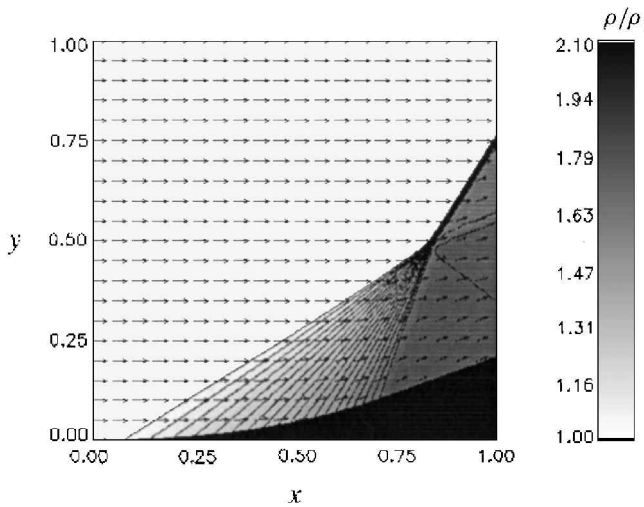

Fig. 10 Perfect gas wave field for a compressive ramp; M_∞ = 2.0, θ_r = 20 deg, SP1 conditions.

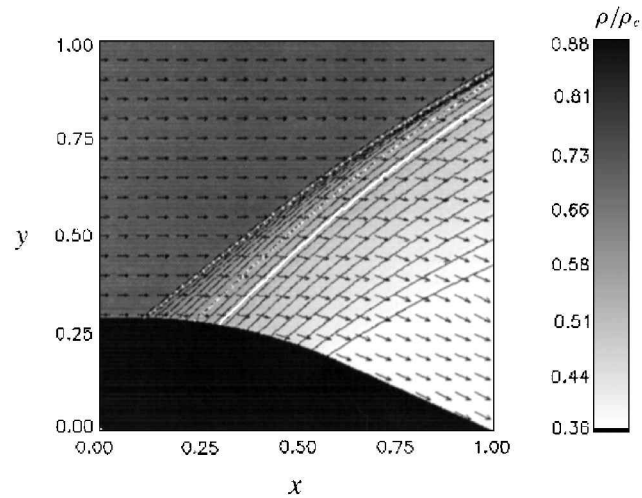

Fig. 11 Dense gas wave field for an expansive ramp; M_∞ = 2.0, θ_r = − 25 deg, SD1 conditions.

slipstream is not distinguishable in the density plot. (Ben-Dor[26] is an excellent source for the theory of classical shock reflections).

A compression fan for the TD1 case on a $\theta_w = 30$ deg compressive wedge is shown in Fig. 3. Although the wave starts to the left of the wedge as a discontinuity, the compression spreads while propagating to the right because the conditions both upstream and downstream of the wave lie in the $\Gamma < 0$ thermodynamic region. The wave spreads because the speed of sound decreases through the wave, which is counter to that of a compression shock. The reflected wave, however, consists of a composite fan–shock wave. Here the gas is compressed out of the $\Gamma < 0$ region, evident by the $\Gamma > 0$ region below the white $\Gamma = 0$ contour line. This allows the formation of the compression shock.

Figure 4 shows an expansion shock incident upon a $\theta_w = 30$ deg wedge for the TD2 conditions. As the shock propagates to the right at $M_I = 1.05$ into the high-density quiescent gas, the fluid travels to

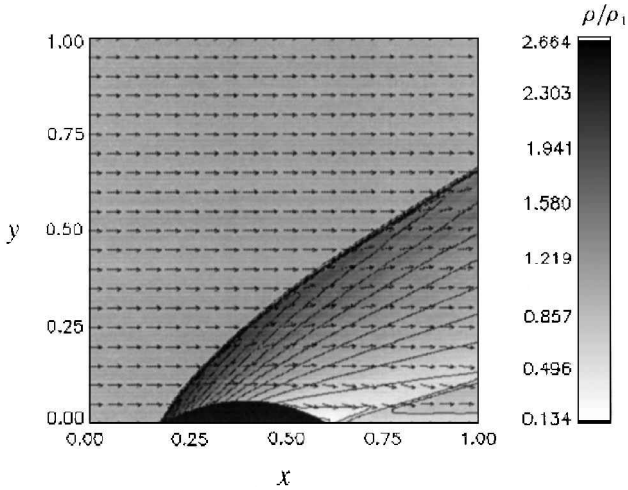

Fig. 12 Steady flow over a circular arc for a perfect gas; $M_\infty = 3.0$, SP1 conditions.

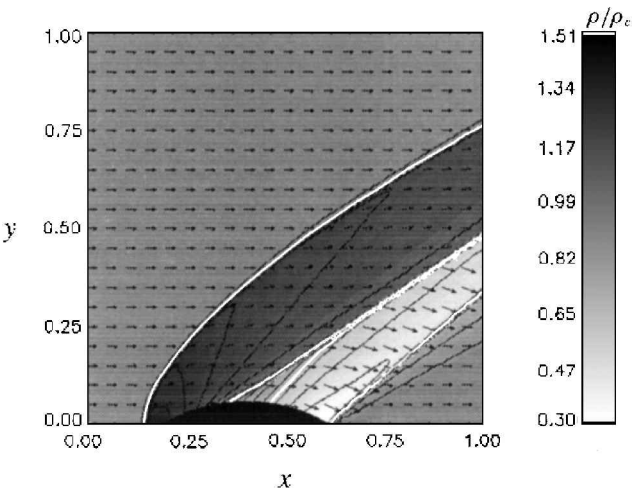

Fig. 13 Steady flow over a circular arc for a dense gas; $M_\infty = 2.0$, SD2 conditions.

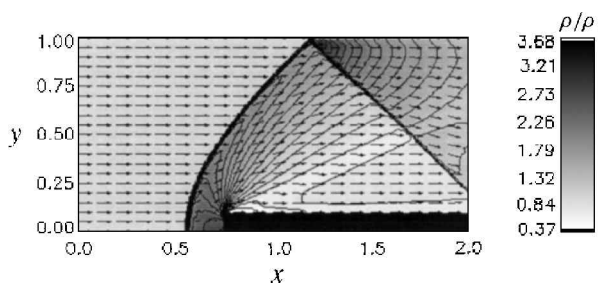

Fig. 14 Forward-facing step for a perfect gas; $M_\infty = 3.0$, SP1 conditions.

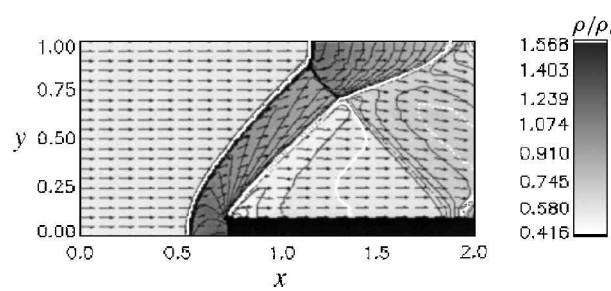

Fig. 15 Forward-facing step for dense gas; $M_\infty = 1.5$, SD2 conditions.

the left upon expanding through the shock so that the left boundary is an outflow boundary. The gas near the wedge at $x = 0.9$ is expanded to a lower density than that farther above the wedge. The gas near the wedge is then recompressed through a compression shock at $x = 0.85$ that emanates from the surface and becomes continuously weaker above the ramp. As expected, the compression shock lies within the $\Gamma > 0$ region generated by the reflection of the expansion shock on the wedge.

Density and velocity fields for moving shock waves refracting over a backward-facing step are shown in Figs. 5–7. A perfect gas compression shock with TP2 conditions and $M_I = 3.2$ is shown in Fig. 5. As the incident shock curves around the step, an expansion fan forms at the corner. The postshock Mach number is supersonic so that no disturbances propagate upstream. Also, an embedded compression forms to the right of the step at $x = 1.2$, $y = 0.4$. This complicated wave field closely matches experimental observations, e.g., Ref. 27.

Case TD3 (Fig. 6) displays a dense gas compression shock with $M_I = 1.23$ and $\Gamma < 0$ behind the shock. An expansion shock is attached to the corner of the step rather than the expansion fan seen in the perfect gas case of Fig. 5. The $\Gamma = 0$ contour indicates that the gas is expanded into the $\Gamma > 0$ region. An expansion shock wave with $M_I = 1.05$ for the TD2 case is shown in Fig. 7. As the shock curves around the step, it spreads into a fan. The only $\Gamma > 0$ region occurs just downstream (note the flow is right to left over the step) of the step at $x = 0.95$.

Steady Flows

Steady, perfect gas and dense gas flowfields are compared in Figs. 8–15. Conditions for all perfect gas cases correspond to SP1. An oblique compression shock attached to a compressive wedge of $\theta_w = 20$ deg with a freestream Mach number $M_\infty = 3.0$ for a perfect gas is shown in Fig. 8. The density ratio downstream of the shock $\rho/\rho_\infty = 2.26$ matches that predicted by theory, e.g., Ref. 28, with an absolute error on the order of 10^{-3}.

The freestream condition for dense gas case SD1 in Fig. 9 lies in the $\Gamma < 0$ region. The wedge is expansive with $\theta_w = -20$ deg. A supersonic flow for a perfect gas over this geometry results in a Prandtl–Meyer expansion fan centered at the corner. The isopycnics in Fig. 9, however, depict an expansion shock–fan combination centered on the corner. The flow is expanded into the $\Gamma > 0$ region through the shock and continues to expand through the fan. The expansion shock reflects from the upper boundary as a fan and intersects the fan from the lower boundary. Note that the velocity vectors turn away from the shock, which is the opposite of what occurs with an oblique compression shock.

A centered compression fan focusing into a compression shock for a perfect gas is shown in Fig. 10. The wave field agrees with the analytical solution derived by Emanuel.[29] The contour of the compressive ramp is calculated for $M_\infty = 2.0$, $\gamma = 1.4$, a focal point of $y = 0.5$, and a terminal ramp angle of $\theta_r = 20$ deg. The fan and primary shock wave intersect at the focal point with a slipstream and a weak secondary oblique shock.

A dense gas flow over an expansive ramp of $\theta_r = -25$ deg is shown in Fig. 11. The freestream Mach number is $M_\infty = 2.0$ with the SD1 conditions such that $\Gamma < 0$ in the freestream. As anticipated, the expansion fan converges away from the lower boundary as indicated by the isopycnics. Once the flow is expanded into the $\Gamma > 0$ region, the fan spreads. The focal point at which the fan converges into an expansion shock lies outside the computational domain. Note that the rate of convergence of the isopycnics is greatest in the region between the two dotted-white $\Gamma < 0$ contours where Γ goes through a minimum. However, just upstream of the $\Gamma = 0$ contour the isopycnics converge much more slowly, indicating the influence of the value of Γ on the rate at which waves spread or converge.

Steady flows over circular arcs are shown in Figs. 12 and 13. For the perfect gas case with $M_\infty = 3.0$ in Fig. 12, the shock is attached to the leading edge of the arc. Flow behind the leading-edge shock expands through a fan over the top of the arc before encountering a secondary shock at the trailing edge of the arc. The SD2 conditions with $M_\infty = 2.0$ result in a detached bow shock upstream of the arc that compresses the flow into the $\Gamma > 0$ region shown in Fig. 13. The expansion fan converges into an expansion shock,

which expands the flow completely through the $\Gamma < 0$ region as evident by the $\Gamma = 0$ contours. This phenomenon is consistent with the theory of Thompson and Lambrakis,[1] which predicts expansion shock formation where Mach lines converge with decreasing pressure and $\Gamma < 0$. The wave at the trailing edge of the arc is shown to consist of a shock–fan composite wave because a portion of the compression across the wave occurs in the $\Gamma < 0$ region.

The wave field with a forward-facing step for a perfect gas with $M_\infty = 3.0$ is shown in Fig. 14. The detached bow shock terminates into a Mach reflection at the upper boundary, indicating a small region of subsonic flow behind the Mach stem. The reflected oblique shock exits at the outflow boundary. Also present is an expansion fan centered at the corner of the step.

Figure 15 shows the dense gas wave field for case SD2 with the same step as that of Fig. 14. The freestream Mach number is $M_\infty = 1.5$, and $\Gamma < 0$ in the freestream. Similar to the perfect gas case, a detached bow shock terminates into a Mach reflection at the upper boundary, compressing the flow into the $\Gamma > 0$ region. The wave centered on the corner of the step takes the form of an expansion fan–shock. As indicated by the double $\Gamma = 0$ contour emanating from the corner, the expansion shock completely expands the flow through the $\Gamma < 0$ region. Also interesting is that the reflected oblique compression shock spreads into a compression fan in the $\Gamma < 0$ region downstream of the expansion shock.

Summary and Conclusions

Two-dimensional wave fields are simulated for an inviscid van der Waals gas representative of heavy fluorocarbons with high specific heats and conditions near the thermodynamic critical point. For selected geometries, the dense gas flowfields are compared with simulations of well-known perfect gas flowfields. The wave structures for shock reflections and refractions in the dense gas regime are found to be significantly different from those of perfect gas flows over similar geometries, for both transient and steady state. Wave structures are consistent with the inviscid theory with respect to the sign of the fundamental derivative, i.e., expansion fans converge into shocks and compression shocks spread into fans in regions where $\Gamma < 0$.

Because the $\Gamma < 0$ region is restricted to a finite range of temperatures and pressures, flowfields containing regions of mixed nonlinearity result in wave configurations that are much more complex than those with either complete positive or negative nonlinearity. Regions of mixed nonlinearity often result in composite waves such as shock–fan or fan–shock combinations.

Simulations such as those presented here will provide a basis for an experimental program to verify the existence of nonclassical, dense gas phenomena. Of course, accurate simulations require a more advanced gas model than the van der Waals model used in the present study. For example, turbine cascade simulations using the Martin–Hou equation of state have been completed. Evidently, turbomachinary designs will soon appear that take advantage of the nonclassical, dense gas dynamics of BZT fluids.

Acknowledgment

This work was sponsored by the National Science Foundation under Grant Number CTS-9614207.

References

[1]Thompson, P. A., and Lambrakis, K. C., "Negative Shock Waves," *Journal of Fluid Mechanics*, Vol. 60, Pt. 1, 1973, pp. 187–208.

[2]Cramer, M. S., "Negative Nonlinearity in Selected Fluorocarbons," *Physics of Fluids A*, Vol. 1, No. 11, 1989, pp. 1894–1897.

[3]Cramer, M. S., "Nonclassical Dynamics of Classical Gases," *Nonlinear Waves in Real Fluid*, edited by A. Kluwick, Springer, New York, 1991, pp. 91–145.

[4]Bethe, H. A., "The Theory of Shock Waves for an Arbitrary Equation of State," Office of Scientific Research and Development, Rept. 545, Washington, DC, June 1942.

[5]Zel'dovich, Y. B., "On the Possibility of Rarefaction Shock Waves," *Zhurnal Eksperimentalnoi i Teoreticheskoi Fiziki*, Vol. 4, 1946, pp. 363, 364 (in Russian).

[6]Thompson, P. A., "A Fundamental Derivative in Gas Dynamics," *Physics of Fluids*, Vol. 14, No. 9, 1971, pp. 1843–1849.

[7]Cramer, M. S., "Steady, Isentropic Flows of Dense Gases," *Physics of Fluids A*, Vol. 3, No. 1, 1991, pp. 219–226.

[8]Aldo, A. C., and Argrow, B. M., "Dense Gas Flow in Minimum Length Nozzles," *Journal of Fluids Engineering*, Vol. 117, No. 2, 1995, pp. 270–276.

[9]Schnerr, G. H., and Molokov, S., "Exact Solutions for Transonic Flows of Dense Gases in Two-Dimensional and Axisymmetric Nozzles," *Physics of Fluids*, Vol. 6, No. 10, 1994, pp. 3465–3472.

[10]Schnerr, G. H., and Leidner, P., "Two-Dimensional Nozzle Flow of Dense Gases," American Society of Mechanical Engineers, Paper 93FE8, June 1993.

[11]Chandrasekar, D., and Prasad, P., "Transonic Flow of a Fluid with Positive and Negative Nonlinearity Through a Nozzle," *Physics of Fluids A*, Vol. 3, No. 3, 1991, pp. 427–438.

[12]Kluwick, A., "Transonic Nozzle Flow of Dense Gases," *Journal of Fluid Mechanics*, Vol. 247, 1993, pp. 661–688.

[13]Anderson, W. K., "Numerical Study on Using Sulphur Hexafluoride as a Wind Tunnel Test Gas," *AIAA Journal*, Vol. 29, No. 12, 1991, pp. 2179, 2180.

[14]Curran, H. M., "Use of Organic Working Fluids in Rankine Engines," *Journal of Energy*, Vol. 5, No. 4, 1991, pp. 218–223.

[15]Maizza, V., "The Use of Unconventional Fluids for Single Stage Supersonic Turbines of Low Power Output," Intersociety Energy Conversion Engineering Conf., Paper 769203, Aug. 1976.

[16]Cramer, M. S., Tarkenton, L. M., and Tarkenton, G. M., "Critical Mach Number Estimates for Dense Gases," *Physics of Fluids A*, Vol. 4, No. 8, 1992, pp. 1840–1847.

[17]Cramer, M. S., and Tarkenton, G. M., "Transonic Flows of Bethe–Zel'dovich–Thompson Fluids," *Journal of Fluid Mechanics*, Vol. 240, 1992, pp. 197–228.

[18]Brown, B. P., "Two-Dimensional Dense Gas Dynamics," Ph.D. Thesis, Univ. of Colorado, Boulder, CO, July 1997.

[19]Monaco, J. F., Cramer, M. S., and Watson, L. T., "Supersonic Flows of Dense Gases in Cascade Configurations," *Journal of Fluid Mechanics*, Vol. 330, 1997, pp. 31–59.

[20]Schnerr, G. H., and Leidner, P., "Numerical Investigation of Axial Cascades for Dense Gases," Proceedings of the Pacific International Conf. on Aerospace Science and Technology, Paper PICAST-1, Taiwan, ROC, 1993.

[21]Borisov, A. A., Borisov, Al. A., Kutateladze, S. S., and Nakoryakov, V. E., "Rarefaction Shock Wave Near the Critical Liquid–Vapour Point," *Journal of Fluid Mechanics*, Vol. 126, 1983, pp. 59–73.

[22]Argrow, B. M., "Computational Analysis of Dense Gas Shock Tube Flow," *Shock Waves*, Vol. 6, No. 4, 1996, pp. 241–248.

[23]Brown, B. P., and Argrow, B. M., "Two-Dimensional Shock Tube Flow for Dense Gases," *Journal of Fluid Mechanics*, Vol. 349, 1997, pp. 95–115.

[24]Emanuel, G., *Advanced Classical Thermodynamics*, AIAA Education Series, AIAA, Washington, DC, 1988, Chap. 8.

[25]Davis, S. F., "A Simplified TVD Finite Difference Scheme via Artificial Viscosity," *SIAM Journal on Scientific and Statistical Computing*, Vol. 8, No. 1, 1987, pp. 1–18.

[26]Ben-Dor, G., *Shock Wave Reflection Phenomena*, Springer–Verlag, New York, 1992.

[27]Schardin, H., *Proceedings of the Seventh International Congress on High Speed Photography*, Academic, New York, 1965, pp. 113–119.

[28]Emanuel, G., *Gasdynamics: Theory and Applications*, AIAA Education Series, AIAA, New York, 1986, Chap. 5.

[29]Emanuel, G., "Near-Field Analysis of a Compressive Supersonic Ramp," *Physics of Fluids*, Vol. 25, No. 7, 1982, pp. 1127–1133.

W. Oberkampf
Associate Editor